Continuum and Discrete Modeling of Craze Failure at a Crack Tip in a Glassy Polymer

Y. Sha, C. Y. Hui,* and A. Ruina

Department of Theoretical and Applied Mechanics, Cornell University, Ithaca, New York 14853

E. J. Kramer

Department of Materials Science and Engineering and the Materials Science Center, Cornell University, Ithaca, New York 14853

Received September 29, 1994; Revised Manuscript Received January 19, 1995[⊗]

ABSTRACT: The problem of craze failure near the tip of a crack embedded inside a craze is investigated by modeling the crazed material as a highly anisotropic network of springs. This model is based on the presence of cross-tie fibrils in the craze microstructure. These cross-tie fibrils give the craze some small lateral load-bearing capacity so that they can transfer stress between the main fibrils. This load transfer mechanism allows the force on the fibril directly ahead of the crack tip in the center of the craze to reach the breaking force of the chain even though the force on a main fibril as it is being drawn at the craze/bulk interface is much lower. When the craze is sufficiently wide, the discrete network model can be approximated as an anisotropic continuum. Explicit expressions are derived which relate the shear and tensile modulus of the crazed material to the underlying microstructural variables such as fibril spacing, fibril diameter and volume fraction. The predictions of the continuum model are compared with those of the discrete model. We focus on the case of a thin craze where the continuum approximation is shown to be inadequate. The results of our model are used to predict the molecular weight dependence of the fracture toughness of polymer glasses, fracture toughness of diluted entanglementt networks, and the kinetics of polymer welding.

1. Introduction

The fracture properties of most polymer glasses are linked to the stress-induced growth and breakdown of crazes, which are planar cracklike defects. However, unlike cracks, crazes are load bearing as their surfaces are bridged by many fine (5−30 nm diameter) fibrils. As the craze grows in width, this fibril structure may break down, leading to large voids inside the craze which eventually grow to become cracks. The process of craze width growth and craze fibril breakdown are thus central to an understanding of the fracture mechanics of polymer glasses.

The best current micromechanics model for the growth of fibrils during craze widening is that of surface drawing; i.e., the craze grows in width by drawing new polymer material into the fibrils from a thin, strain-softening layer at the craze−bulk interface ("the active zone").[1] The width of this active zone is on the order of the fibril diameter and can be observed using a gold decoration technique.[2] Measurements of craze widening ahead of cracks have been made using transmission electron microscopy (TEM) and optical interference techniques.[3] From the amount of craze widening, the continuum stress acting in a direction normal to the craze−bulk interface can be deduced.[4] This drawing stress σ_d is found to be practically uniform along the entire length of the craze, with the exception of a very small region near the crack tip. In this region, there is a stress concentration which is difficult to quantify due to the limited resolution of optical microscopy and TEM.

The micromechanics of craze breakdown are not as well understood. One theory is that craze breakdown occurs by localized creep along the fibrils.[5] If this hypothesis were true, one would expect to see that voids nucleated most frequently in the midrib, the oldest portion of the craze which has a somewhat higher extension ratio than the rest due to its being drawn in the high-stress zone just behind the craze tip. However, recent morphological observations,[6,7] show that all the fibril breakdowns initiate at the craze−bulk interface. It should be noted that chain scission accompanying fibril surface formation at the bulk−craze interface alone is not sufficient to cause craze breakdown[8] so that fibril breakdown along the interface requires a loss of entanglement density. Indeed, a model of fibril failure based on chain scission and entanglement loss during the drawing process has led to satisfactory agreement with experimental results.[8] It should be noted that the craze breakdown results stated above correspond to the process of crack initiation in a defect-free craze. Such cracks, once initiated, grow by failure of the fibril structure directly ahead of their tips. A mechanism of such craze failure at a crack tip has been proposed by Brown.[9] Before Brown's work, the craze fibrils were always modeled as straight parallel cylinders aligned along the normal to the craze surfaces and running from one craze interface to another. However, transmission electron microscophs and electron diffraction show the existence of short fibrils running between the main fibrils.[10,11] A model for the microstructure of the cross-tie fibrils is shown in Figure 1. These "cross-tie" fibrils give the craze some small lateral load-bearing capacity so that they can transfer stress between the main fibrils.[9] Brown[9] pointed out that this load transfer mechanism allows the normal stresses on the fibrils directly ahead of the crack tip to reach the breaking stress of the chains. On the basis of Brown's approach, Hui et al.[12] developed an approximate analytical model to examine the effect of various stress boundary conditions at the craze−bulk interface. In neither of these papers[9,12] was there a serious attempt to relate the underlying microstructure of the craze to the continuum

[⊗] Abstract published in *Advance ACS Abstracts,* March 1, 1995.

0024-9297/95/2228-2450$09.00/0

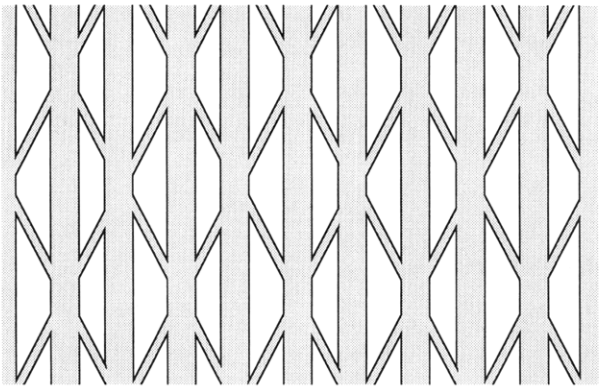

Figure 1. Schematic of craze microstructure.

moduli. Furthermore, neither work examined the case of a thin craze, where the continuum model is expected to break down. Such thin crazes are formed along interfaces in the early stage of crack healing, for example.

In this work we outline a general method to relate the continuum moduli of the crazed material to its microstructure. Explicit closed form expressions are derived which relate the moduli to the fibril volume fraction and fibril modulus for a spring network model microstructure which approximates the properties of an actual craze. We numerically compute the deformation of the discrete network model and compare the results with those from the continuum model. In particular, we focus on the case of a thin craze where the continuum model becomes inaccurate.

Spring network models have been used extensively to study brittle failure of elastic materials.[13-20] Network models have also been used to study more explicitly the effects of material microstructures on fracture.[21-28] A comprehensive review of the spring network and finite element model for elasticity and fracture can be found in Jagota.[29] Jagota found that in problems (problems of type **P1** in ref 29) where the discreteness of the model matches the discreteness of the material, the spring network models are valid and appropriate. However, in problems where the spring network is being used as a discretization of a continuum (problems of type **P2** in ref 29), Jagota pointed out that there are deficiencies, as models of both elasticity and fracture. In this work the spring network is used to model the discrete microstructures of the craze so that they belong to that of type **P1**. We also note that Xiao and Curtin[30] have recently employed the spring network model to study the initiation, propagation, and subsequent breakdown of a craze in a bulk polymer. Using a network model of a craze that is different than the network model used in this work, their numerical simulation showed qualitative agreement with the continuum models proposed by Brown[9] and Hui et al.[12] In this paper, we use a network model that matches the discreteness of the craze microstructures so that we can investigate the limitations of the continuum crack tip model proposed by Brown.[9] We have not, as Xiao and Curtin[30] have done, investigated the initiation and propagation of the craze.

2. Spring Network Model

The craze is modeled by a two-dimensional periodic network of linear springs. A two-dimensional network will suffice since the craze is to be loaded under plane strain conditions so that the deformation field is independent of the out-of-plane coordinate z. Due to periodicity, the network can be formed by translation of a unit cell. A special case of such a network with its unit cell is shown in Figure 2. This network models the craze microstructures in Figure 1. The springs which model the main fibrils have spring constant k_m whereas the cross-tie fibrils have spring constant k_c. The distance between the main fibrils is denoted by d, and the angle between the cross-tie fibrils and main fibrils is denoted by θ. The cross-section areas (and lengths) of the main fibrils and the cross-tie fibrils are denoted by A_m and A_c (l and l_c), respectively.

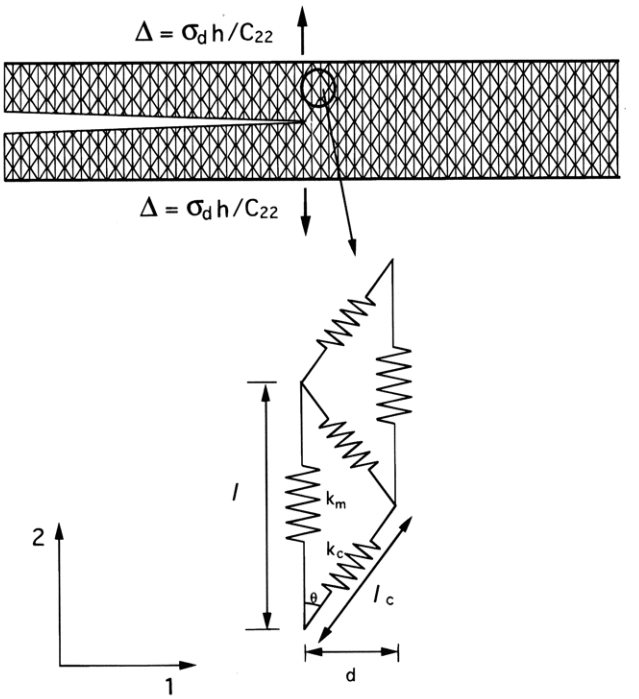

Figure 2. (a, top) Schematic diagram showing the discretization of the craze microstructure in Figure 1 using a periodic spring network; also the geometry and boundary conditions of the micromechanics problem. A uniform displacement $\sigma_d h/C_{22}$ is applied on the craze–bulk boundary in the direction parallel to the main fibrils so that the normal stress on the craze–bulk boundary is equal to the drawing stress σ_d at sufficiently large distances away from the crack tip. (b, bottom) A unit cell of the periodic spring network. l and d are the length and spacing of the main fibrils respectively. k_m and k_c are the spring constants of the main and cross-tie fibrils, respectively.

The continuum moduli of such networks are obtained by imposing a spatially homogeneous affine transformation to the network; i.e., let $\mathbf{X}$ denote the position vector of a generic node of the network, as shown in Figure 2. The position of this node $\mathbf{x}$ after an affine transformation is

$$\mathbf{x} = \mathbf{X} + \mathbf{L}\cdot\mathbf{X} = \mathbf{X} + \mathbf{u} \tag{1}$$

where $\mathbf{L}$ is a second-order tensor. The deformation of the network is characterized by the deformation gradient $\mathbf{F} = \mathbf{I} + \mathbf{L}$, where $\mathbf{I}$ is the identity tensor. In the continuum limit, the average strain ϵ_{ij} is

$$\epsilon_{ij} = (u_{i,j} + u_{j,i})/2 \qquad i,j = 1, 2 \tag{2}$$

where we have assumed small strain theory and the u_i's are the Cartesian components of the vector $\mathbf{u}$. In the continuum limit, the average stress σ_{ij} is defined as

$$\sigma_{ij} = \frac{1}{V_{cell}} \int_{V_{cell}} \sigma_{ij}' \, dV \tag{3a}$$

where $V_{cell} = d^2 l$ is the volume of a unit cell which has a thickness d in the z direction. σ_{ij}' is the stress on each fibril in the unit cell. Let f_{ik} be the ith Cartesian component of the resultant force acting on the kth node ($i, j = 1, 2$ and $k = 1-4$) which is located at X_{jk}, where X_{jk} is the jth Cartesian coordinate of the kth node. Using (3a), σ_{ij} is found to be

$$\sigma_{ij} = \frac{1}{V_{cell}} f_{ik} X_{jk} \tag{3b}$$

where the summation convention over repeated indexes is used.

For a given arbitrary u_i or ϵ_{ij}, the stretch of each of the springs in a unit cell can be computed from purely kinematic considerations. The force on each spring can be computed on the basis of the constitutive model for the springs. In our case the springs are linear so that the spring forces are directly proportional to the stretches via the spring constants k_m and k_c; i.e., the spring forces can be expressed in terms of the unit cell geometry and ϵ_{ij}. This procedure allows us to express the average stress σ_{ij} in terms of the average strain ϵ_{ij} using (3b). For the special case shown in Figure 2, the stress–strain relation is found to be

$$\begin{aligned} \sigma_{11} &= C_{11}\epsilon_{11} + C_{12}\epsilon_{22} \\ \sigma_{22} &= C_{12}\epsilon_{11} + C_{22}\epsilon_{22} \\ \sigma_{12} &= 2C_{66}\epsilon_{12} \end{aligned} \tag{4a}$$

where the constants C_{ij} are defined by

$$C_{11} = \mathscr{E}_c \sin^4\theta \qquad C_{12} = \mathscr{E}_c \sin^2\theta \cos^2\theta$$

$$C_{22} = \mathscr{E}_m + \mathscr{E}_c \cos^4\theta \qquad C_{66} = C_{12} \tag{4b}$$

where E_m (E_c) is the effective modulus of the main (cross-tie) fibrils and is defined by

$$\mathscr{E}_m = v_m E_m = v_m k_m l / A_m \tag{4c}$$

and

$$\mathscr{E}_c = v_c E_c = v_c k_c l_c / A_c \tag{4d}$$

where l and l_c denote the length of main and cross-tie fibrils, respectively. In (4c) and (4d), $E_m = k_m l / A_m$ is the extensional modulus of a typical main fibril and $E_c = k_c l_c / A_c$ is the extensional modulus of a typical cross-tie fibril. Let V_m and V_c denote the volumes occupied by the main and cross-tie fibrils in a unit cell, then $v_m = V_m / V_{cell}$ and $v_c = V_c / V_{cell}$ are the volume fractions of the main fibrils and the cross-tie fibrils, respectively. In particular, for $\theta \ll 1$, we have

$$\begin{aligned} C_{11}/C_{66} &= \theta^2 \\ C_{12}/C_{66} &= 1 \end{aligned} \tag{4e}$$

$$C_{22}/C_{66} = (1 + \varrho)/\varrho\theta^2 \quad \text{and} \quad C_{22} = \mathscr{E}_m + \mathscr{E}_c$$

where $\varrho = \mathscr{E}_c / \mathscr{E}_m$.

The matrix C_{ij} can be inverted to give the relation between strain and stress, i.e.,

$$\begin{aligned} \epsilon_{11} &= a_{11}\sigma_{11} + a_{12}\sigma_{22} \\ \epsilon_{22} &= a_{12}\sigma_{11} + a_{22}\sigma_{22} \\ 2\epsilon_{12} &= a_{66}\sigma_{12} \end{aligned} \tag{5a}$$

where a_{ij} are

$$\begin{aligned} a_{11} &= [\mathscr{E}_c \sin^4\theta]^{-1} + \cos^4\theta [\mathscr{E}_m \sin^4\theta]^{-1} \\ a_{12} &= -\cos^2\theta [\mathscr{E}_m \sin^2\theta]^{-1} \\ a_{22} &= 1/\mathscr{E}_m \\ a_{66} &= [\mathscr{E}_c \sin^2\theta \cos^2\theta]^{-1} \end{aligned} \tag{5b}$$

In particular, for $\theta \ll 1$, we have, approximately

$$\begin{aligned} a_{11}/a_{66} &= (1 + \varrho)/\theta^2 \\ a_{12}/a_{66} &= -\varrho = -\mathscr{E}_c/\mathscr{E}_m \\ a_{22}/a_{66} &= \varrho\theta^2 \end{aligned} \tag{5c}$$

Brown, in his work,[9] assumed that $a_{11} \sim a_{66}$, which is inconsistent with the results for our craze model which states that $a_{66}/a_{11} = O(\theta^2)$. All the equations in Brown[9] for craze failure are correct if his E_1 is replaced by C_{66}.

Using $l = 60$ nm, $\theta = 30°$, $v_m = 0.225$, $v_c = 0.0255$, and $E_m = E_c = 3$ GPa, the C_{ij}'s are found to be $C_{11} = 4.8$ MPa, $C_{22} = 7.2 \times 10^2$ MPa, and $C_{12} = C_{66} = 14$ MPa, respectively. $\theta = 30°$ implies that the spacing d between the main fibrils is 17.3 nm. While these numbers are thought to be appropriate for polystyrene (PS) from the work of Miller et al.,[10] considerable uncertainties exist in v_m and v_c, although their sum, the total fibril volume fraction in the craze, has been experimentally measured by TEM. Similarly, the assumption that $E_m = E_c = E$, the Young's modulus of the unoriented polymer, is at least questionable.[31] Finally, while $\theta = 30°$ gives roughly the correct interfibril spacing for PS, the real fibril structure differs significantly from that of the idealized spring network model.[10] Nevertheless, this simple spring network model of the craze will give us a way to check the approximations of the continuum model.

3. Governing Equations for the Continuum Model

The continuum constitutive description of a craze (4) can be incorporated into a continuum model of the craze zone. If one assumes the validity of the continuum hypothesis, the governing equation for the stress field in the craze for the case of plane strain deformation with respect to a fixed Cartesian coordinate system (x, y) is[32]

$$a_{11}\phi_{,2222} + [2a_{12} + a_{66}]\phi_{,1122} + a_{22}\phi_{,1111} = 0 \tag{6a}$$

where $,_1$ and $,_2$ denote partial derivatives with respect to x and y respectively. ϕ is the scalar stress function defined by

$$\sigma_{ij} = \phi_{,kk}\delta_{ij} - \phi_{,ij} \tag{6b}$$

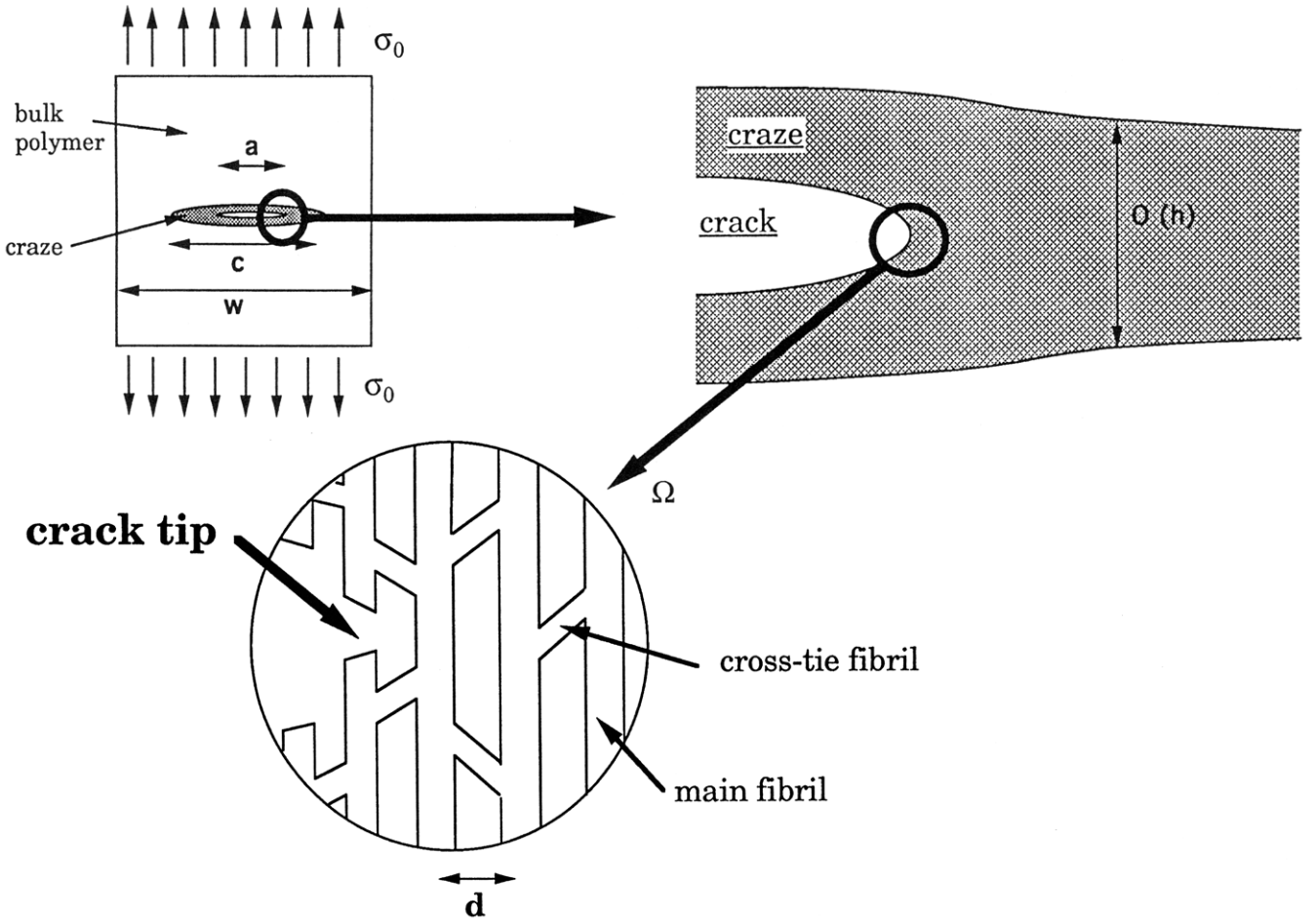

Figure 3. (a, top) Schematic diagram showing the geometry of a crack inside a craze under external loading. (b, bottom) Schematic diagram focusing on the area of interest Ω which is embedded in a region of length scale of order h, the length of the drawn fibrils inside the craze.

When $C_{11}/C_{66} \ll 1$ and $C_{66}/C_{22} \ll 1$, it was proposed by Hui et al.[12] that the deformation field in the craze can be approximated by the simpler equation

$$V_{,XX} + V_{,YY} = 0 \tag{7}$$

where

$$X = x/(h\alpha)$$
$$Y = y/h \tag{8}$$
$$V = v/h$$

where v is the displacement in the y direction and α^2 is a dimensionless material constant defined by

$$\alpha^2 = C_{66}/C_{22} \tag{9a}$$

It should be noted that the notation C_{66} in this work corresponds to the notation C_{12} in Hui et al.[12] In deriving (7) and (9b), the stress component σ_{xx} and the displacement u in the x direction are neglected. In this approximation, σ_{12} and σ_{22} are related to V by

$$V_{,Y} = v_{,2} = \sigma_{22}/C_{22} \qquad V_{,X} = \alpha v_{,1} = \sigma_{12}/C_{22}\alpha \tag{9b}$$

and the traction free boundary condition on the crack faces reduces to

$$\sigma_{22} = 0 \quad Y = 0 \quad \text{and} \quad X < 0 \tag{9c}$$

Later, it will be shown that the stress field calculated using (7)–(9) is an excellent approximation to (6) under the conditions stated above.

4. Boundary Conditions

One of the difficulties in modeling the process of fibril breakdown near the tip of a crack inside the craze zone is the specification of the boundary conditions. The geometry of a crack inside a craze under external loading is illustrated schematically in Figure 3a. Figure 3b focuses on the area of interest Ω which is embedded in a region of length scale of order h, the half-width of the craze. A typical length scale for Ω is d, the fibril spacing. Let a be the crack length, c the length of the craze + crack, and w a typical dimension of the specimen. Then, in general,

$$w > c > a \gg h \gg d \tag{10}$$

The inequality $c > a \gg h$ allows us to model the crack and craze as infinite in extent with respect to h, as shown in Figure 3. Since the thickness of the bulk–craze interface is much less than d, it is represented as a line (the external boundary of the strip) in Figure 2. The material inside the strip consists of drawn main fibrils and cross-tie fibrils connecting them and can be modeled as a linear anisotropic elastic material for a sufficiently thick craze. The difficulty lies in the specification of boundary conditions on the exterior boundary of the strip since the boundary traction depends on the fibril drawing process at the craze–bulk interface as well as the deformation response of the

cross-tie fibrils inside the strip. In the following analysis we shall follow Brown[9] who prescribed a uniform displacement $v = \Delta = \sigma_d h/C_{22}$ on the strip boundary where σ_d is the drawing stress.

5. Results of the Continuum Model

An exact solution of (7) can be obtained using the displacement boundary condition of Brown,[9] i.e., $v(x, |y| = h) = \Delta = \sigma_d h/C_{22}$. This condition must be supplemented by the traction free boundary condition $\sigma_{22} = 0$ on the crack faces at $y = 0, x < 0$. $\sigma_{22}(x, y)$ is found to be

$$\sigma_{22} = \sigma_d \,\mathrm{Re}[1 - \exp(-\pi(X + iY))]^{-1/2} \qquad (11)$$

where Re denotes the real part of a complex number. In particular, the normal stress $\sigma_{22}(x > 0, y = 0)$ directly ahead of the crack tip is

$$\sigma_{22} = \sigma_d[1 - \exp(-\pi x/h\alpha)]^{-1/2} \qquad (12a)$$

For $x/h\alpha \ll 1$, σ_{22} becomes

$$\sigma_{22} \sim K_{tip}(2\pi x)^{-1/2} \qquad (12b)$$

where

$$K_{tip} = \sigma_d[2\alpha h]^{1/2} \qquad (12c)$$

is the local stress intensity factor. The normal stress acting on the craze–bulk interface at $y = |h|$ is

$$\sigma_{22} = \sigma_d[1 + \exp(-\pi x/h\alpha)]^{-1/2} \qquad (12d)$$

It is important to note that the normal stress on the craze–bulk boundary decays to zero exponentially fast with characteristic distance $h\alpha \ll h$ as one moves away from the crack tip in the negative x direction. The local energy release rate G_{tip} is related to the local stress intensity factor K_{tip} using the approximate solution technique (9) by

$$G_{tip} = [K_{tip}]^2/[2C_{22}\alpha] \qquad (13)$$

For the anisotropic material described by (6), $G_{tip\ exact}$ is related to K_{tip} by[32]

$$G_{tip\ exact} = K_{tip}{}^2[a_{22}/2]^{1/2}\left[a_{22} + \frac{2a_{12} + a_{66}}{2}\right]^{1/2} \qquad (14a)$$

Note that there is a typographical error in Brown's[9] energy expression. The factor $(a_{22}/a_{11})^{1/2}$ in his energy release rate expression should be replaced by a_{22}/a_{11}. For $\theta \ll 1$, using (4e) and (5c), $G_{tip\ exact}$ reduces to

$$G_{tip\ exact} = [K_{tip}]^2[(1 + \varrho)(1 - 2\varrho)]^{1/2}/[2C_{22}\alpha] \qquad (14b)$$

where $\varrho = E_c/E_m$, so that the relative error

$$|G_{tip\ exact} - G_{tip}|/G_{tip} = 1 - [(1 + \varrho)(1 - 2\varrho)]^{1/2} \sim \varrho/2 \qquad (15)$$

for $\varrho \ll 1$. The excellent agreement between the two energy release rates for small ϱ implies that the local stress intensity factor K_{tip} is well approximated by the solution of (7) for the special case of displacement boundary conditions.

For our case, $\theta = 30°$ or 0.5236 radian, so that the condition $\theta \ll 1$ is not really satisfied. However, a direct calculation shows that the stress intensity factor obtained using the exact relation (14a) and $G_{tip\ exact} = \sigma_d{}^2 h/C_{22}$ gives

$$K_{tip} = 1.424\sigma_d[\alpha h]^{1/2} \qquad (16)$$

implying that the percentage error using K_{tip} given by the approximate solution (12c) is 0.7%.

To test the approximate expression for the normal stress distribution directly ahead of the crack tip (12a), we compute for the strip problem the normal stress $\sigma_{22}(x, y = 0)$ directly ahead of the crack tip by solving eq 6a using a finite element method. A comparison of $\sigma_{22}(x, y = 0)$ using the finite element method and the approximate solution (12a) is shown in Figure 4a. For all practical purposes (12a) provides an excellent approximation for the normal stress directly ahead of the crack tip in the anisotropic continuum for *all* $x > 0$. Figure 4b compares the normal stress on the craze–bulk interface (at $y = h$) obtained using the finite element method and the approximate solution (12d). Again, the agreement is good. It should be noted that the exact angular dependence of the stress distribution

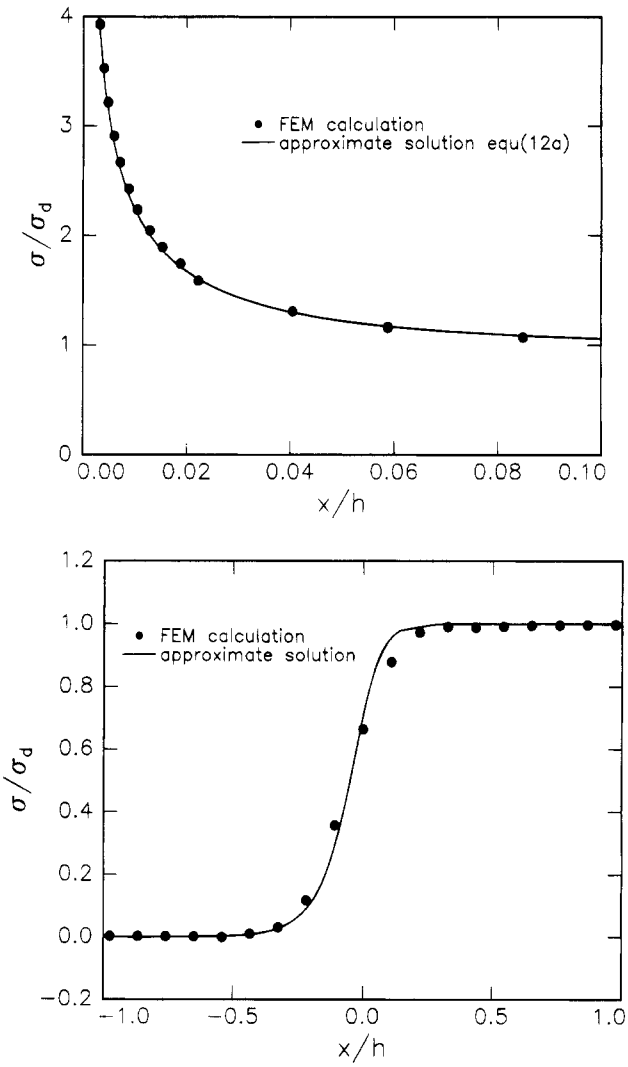

Figure 4. (a) $\sigma_{22}(x, y = 0)/\sigma_d$ obtained using the finite element method (i.e., the numerical solution of (6a)) versus the approximate solution (12a). x/h is the normalized distance directly ahead of the crack tip which is located at $x = 0$. Figure 4b compares the normal stress $\sigma_{22}(x, y = h)/\sigma_d$ on the craze–bulk interface at $y = h$ obtained using the finite element method and the approximate solution (12d).

near the crack tip and away from the cracked plane may still not be well approximated by (11).

6. Fracture Criterion

In the discrete model we assume that crack growth occurs when the force on the fibril immediately ahead of the crack tip reaches the fibril breaking force $F_b = n_e f_b$, where n_e is the number of load-bearing entangled polymer strands in a typical main fibril and f_b is the force required to break a polymer backbone.

In the continuum model of craze failure, the above failure criterion is replaced by the stress-based fracture criterion[9,12]

$$\sigma_{22}(x = D, y = 0) = \sigma_f = \Sigma_{eff} f_b \tag{17}$$

where Σ_{eff}, the number of entangled strands per nominal unit craze area, is given by[8]

$$\Sigma_{eff} = q\Sigma[1 - (M_e/qM_n)] \tag{18}$$

where Σ is the areal density of entangled strands which cross a plane in the undeformed polymer glass. This nominal area is normal to the main craze fibrils; no correction is made for the void volume fraction within the craze. M_e is the entanglement molecular weight (determined from the shear modulus on the rubber plateau above the glass transition temperature T_g) and M_n is the number average molecular weight of the polymer before crazing. The factor $(1 - M_e/qM_n)$ is a correction factor for the chain end segments which cannot form part of the entanglement network but are also accounted for in the entanglement density v_e which is related to Σ by $\Sigma = v_e d_e/2$[1] where d_e, the root mean square end to end distance between entanglments, is a measure of the mesh size of the entanglement network. In our model, $\Sigma_{eff} = n_e d^{-2}$ since d^{-2} is the number of main fibrils per unit nominal area.

The characteristic distance D is treated as an unknown parameter in the continuum theory but is anticipated to be of the order of the fibril spacing. D will be determined in a later section using the results of the discrete model. In order for the continuum theory to be valid, $D \ll h$ so that (12b) is valid at $x = D$. In this case, the craze fails when

$$K_{tip} = \Sigma_{eff} f_b (2\pi D)^{1/2} \tag{19}$$

Using (12c), the critical craze width $2h_c$ for the onset of crack advance is

$$2h_c = 2\pi D(\Sigma_{eff} f_b)^2/[\sigma_d]^2\alpha \tag{20}$$

The craze width $2h$ is related to the continuum opening displacement δ by[1]

$$\delta = 2h(1 - v_f) \tag{21}$$

where v_f is the volume fraction of the fibrillated material in the craze. The fracture toughness G_c is estimated using the Dugdale model[33] and is

$$G_c = 2\pi D(1 - v_f)(\Sigma_{eff} f_b)^2/(\sigma_d\alpha) \tag{22}$$

Thus the continuum theory based on the crack tip field (12b) predicts that G_c is proportional to Σ_{eff}^2, as first pointed out by Brown.[9]

7. Simulation of the Deformation Field in a Craze Using the Spring Network Model

It is anticipated that continuum model (7) will provide an accurate description of the failure process as long as the craze width $2h$ satisfies the inequality $h \gg d/\alpha$ so that the averaging process described in section 2 is meaningful. In this case, the region of dominance of the K_{tip} field is larger than the fibril spacing so that (12b) is valid. Since $d \sim 20$ nm, the continuum model is likely to fail for crazes thinner than 1 μm. To explore the limitations of the continuum model and to investigate the failure mechanism of a thin craze, we carried out a numerical simulation of the strip model described above where the materials inside the strip is modeled by a discrete network of springs, as shown in Figure 2.

7.1. Determination of *D* in the Continuum Model. The force F_{cct} required to cause the crack tip fibril to fail in the continuum model is

$$F_{cct} = K_{tip}(2\pi D)^{-1/2} d^2 \tag{23}$$

The subscript cct indicates that the force is computed using the asymptotic crack tip stress field (12b). The parameter D is determined by setting F_{cct} equal to $F_D(\infty)$, which is the computed force on the crack tip fibril in the discrete model when $2h/l \to \infty$, i.e.,

$$D = [d^2 K_{tip}/F_D(\infty)]^2/2\pi \tag{24}$$

We estimate $F_D(\infty)$ by solving the discrete model using $2h/l = 50$, which corresponds to a 3 μm thick craze. $D = 0.47d$ if we set F_{cct} equal to $F_D(\infty)$. $D = 0.5d$ if we set $F_{cont} = \sigma_{22}(x = D, y = 0)\, d^2$ equal to $F_D(\infty)$. σ_{22} in F_{cont} is computed using the complete stress field directly ahead of the crack tip (12a).

7.2. Limitations of the Continuum Model. Figure 5 compares the normal stress directly ahead of the crack tip computed using the discrete model with those computed by evaluating the asymptotic K field (12b) and the full field (12a) at $x = D$ for different values of the craze width. The continuum crack tip field model using the asymptotic K field (12c) underestimates the stresses when $2h/l < 10$, while the full field (12a) produces a small overestimate of the stress. Thus, for weak crazes, the continuum model based on the K_{tip} field will not give accurate predictions, especially if the usual asymptotic K field (12c) is used.

To be more specific, we compare F_{cct} in (23) with $F_D(2h/l)$, where $F_D(2h/l)$ is the force on the crack tip fibril in the discrete model for different normalized craze widths $2h/l$. Figure 6 shows the dependence of F_D/F_{cct} on $2h/l$. Note that $F_D/F_{cct} = 1$ exactly at $2h/l = 50$, since D is determined by (24). The continuum model is valid as long as the deviation of F_D/F_{cct} from unity is small. If $F_D/F_{cct} > 1$, use of the continuum crack tip field *overestimates* the critical craze width $2h_c$ needed for crack advance, thus overestimating the fracture toughness.

Note that $2h/l > 3$ in Figures 5 and 6. When $2h < l$, the cross-tie fibrils cannot transfer load to the main crack tip fibril. Crazes having widths less than $3l$ are not fully developed. The fracture toughness of such crazes which fail at such small widths (e.g. due to a very low chain density Σ_{eff}) is less than 10 J/m^2.

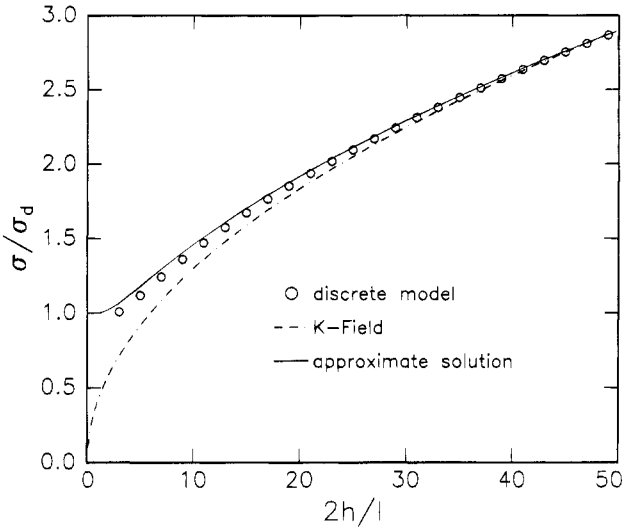

Figure 5. Normal stress directly ahead of the crack tip computed using the discrete model (open circles) compared with the asymptotic K_{tip} field (12b) (dotted line) and the full field (12a) (solid line) for different values of normalized craze width $2h/l$, where l is the length of a typical main fibril. In the discrete model, the normal stress is computed by dividing the force on the crack tip fibril by d^2. In the continuum model, the normal stress is computed by evaluating (12a) and (12b) at $x = D$.

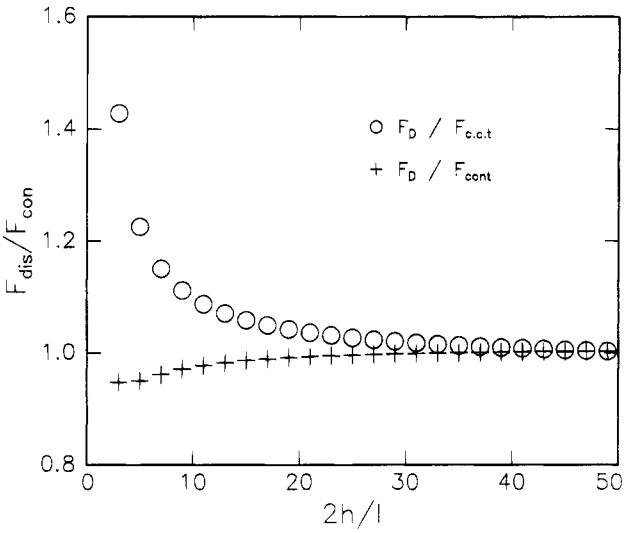

Figure 6. (Upper curve) $F_D(2h/l)/F_{cct}$, where $F_D(2h/l)$ is the force on the crack tip fibril in the discrete model, for different normalized craze widths $2h/l$. The subscript cct in F_{cct} indicates that this force is computed using the asymptotic crack tip stress field (12b). Note that $F_D/F_{cct} = 1$ exactly at $2h/l = 50$ since D is determined by (24). The continuum crack tip field model is valid as long as the deviation of F_D/F_{cct} from unity is small. The lower curve plots $F_D(2h/l)/F_{cont}$, where F_{cont} is computed using the complete stress field directly ahead of the crack tip which includes the singular term (12b) and nonsingular terms. The continuum model is valid as long as the deviation of F_D/F_{cont} from unity is small.

The upper curve in Figure 6 shows that the use of the continuum crack tip (K_{tip}) field leads to a 10% error when $2h/l \sim 18$. At $2h/l = 3$, the error is about 42%. The deviation of F_D/F_{cct} from unity is due to the following: (a) the F_{cct} is computed on the basis of the dominance of the asymptotic field (12b) and (b) the continuum model and the discrete model differ as one approaches the crack tip. To study the limitation of the full continuum model (12a), F_D/F_{cont} is shown as the lower curve in Figure 6, where

$$F_{cont} = \sigma_{22}(x = D, y = 0)d^2$$

Here, F_{cont} is computed using the complete stress field directly ahead of the crack tip which includes the singular term (12b) and nonsingular terms. The full field (12a) underestimates the force on the crack tip fibril and therefore underestimates the fracture toughness. Nevertheless, the full field continuum solution provides a good approximation of the results from the discrete model throughout the *entire* range of craze width. The maximum error made using the full field solution occurs at $2h/l = 3$ and is about 10%.

The continuum crack tip (K_{tip}) field model (22) predicts that the G_c is proportional to Σ_{eff}^2. Figure 7 shows a log–log plot of G_c vs Σ_{eff} resulting from the discrete model, using the following values of the parameters from a craze in PS: $d = 17.3$ nm, $l = 60$ nm, $v_f = 0.25$, $\sigma_d = 55$ MPa, and $f_b = 2 \times 10^{-9}$ N. As before, D is set equal to $d/2$ so that the two models give identical results in the limit of large $2h/l$. Figure 7 is obtained by the following procedure: for each $2h/l$, the force on the crack tip fibril is obtained using the two models (i.e., (23) and Figure 5), these forces are then set equal to $\Sigma_{eff}f_b$, thus determining the chain density Σ_{eff} needed for craze failure. The corresponding fracture toughness G_c is found using $2\sigma_d h(1 - v_f)$. The results show, as expected, that the Σ_{eff}^2 scaling breaks down and is an overestimate for weak (narrow) crazes. The parameter A in Figure 7 can be found using (22) and is

$$A = 2\pi(1 - v_f)Df_b^2/(\sigma_d\alpha)$$

From Figures 6 and 7, we anticipated that the full field solution (12a) should provide a good approximation for the fracture toughness G_c. Using (12a) and (17), G_c is found to be

$$G_c = 2\pi(1 - v_f)\sigma_d D[-\alpha \ln(1 - [\sigma_d/\Sigma_{eff}f_b]^2)]^{-1} \quad (25)$$

The limit $G_c = A\Sigma_{eff}^2$ is recovered when $[\sigma_d/\Sigma_{eff}f_b]^2 \ll 1$ since $\ln(1 - p) \approx -p$ for small p. Figure 7 shows that (25) is a good approximation of the fracture toughness for the entire range of Σ_{eff}.

Discussion

The results obtained above suggest that the full field continuum solution ((12a) and (25)) should be used in estimating the fracture toughness G_c produced by weak crazes at crack tips.

(1) Molecular Weight Dependence of G_c. To illustrate the usefulness of the full field continuum solution ((12a) and (25)), we employ it to compute the molecular weight dependence of G_c in polystyrene (PS) and poly(methyl methacrylate) (PMMA). From (18) Σ_{eff} approaches zero as M_n approaches $q^{-1}M_e$, or about $2M_e \approx M_c$, where M_c is the critical molecular weight for entanglement at which a log–log plot of zero shear rate viscosity of the melt versus M exhibits a change in slope from 1 to ~3.4. It is of course well-known that stable crazes are not observed for $M_n < M_c$. However it is equally well-known that the fracture properties of glassy polymers continue to increase as M_n is increased above M_c; e.g., G_c does not approach an asymptotic value until $M_n \gg M_c$. In this section we use the results above to compute the dependence of G_c on M_n in the regime $q^{-1}M_e < M_n < 10M_c$. Since in the low M_n part of this

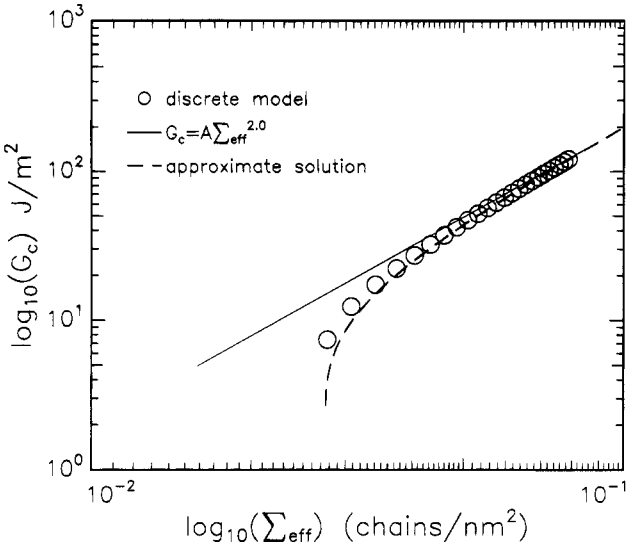

Figure 7. log–log plot of fracture toughness G_c vs effective areal chain density Σ_{eff} within the craze. Open circles are computed from the discrete model, using the following values of the parameters from a craze in PS: d = 17.3 nm, l = 60 nm, v_f = 0.25, σ_d = 55 MPa, and $f_b = 2 \times 10^{-9}$ N. The solid line which has slope = 2 (i.e., $G_c = A\Sigma_{eff}^2$) is based on the continuum crack tip field (12b). The dashed line is the prediction based on (25), which uses the full continuum solution (14a).

range the G_c is quite small and the craze narrow, the full field continuum solution ((12a) and (25)) should be used.

For PS the parameters that enter eq 18 ($\Sigma_{eff} = q\Sigma[1 - (M_e/qM_n)]$) have been previously estimated[11,34] to be $q \approx 0.6$, $\nu_e = 3.5 \times 10^{25}$ strands/m^3, d_e = 9.6 nm, Σ = 0.168 strands/nm^2, and M_e = 18 000, so that Σ_{eff} = 0.101-(1 − 30000/M_n) strands/nm^2. Similar estimates for PMMA[34] give $q \approx 0.63$, $\nu_e = 7.8 \times 10^{25}$ strands/m^3, d_e = 7.3 nm, Σ = 0.285 strands/nm^2, and $M_e \approx 11\,000$. Using the results from the previous section (25), we plot the predicted G_c as a function of M_n for PS in Figure 8 and that for PMMA in Figure 9.

The only parameter which is highly uncertain in our model of the craze structure is the angle θ, which influences α [$=(C_{12}/C_{22})^{1/2}$]. Because the geometry of the spring model is not exactly that of the craze fibril structure, the structural parameters determined previously by TEM for PS[10] and PMMA[11] crazes cannot be used directly to obtain θ. Therefore we have treated θ as a parameter and plot curves for several different values of θ in Figures 8 and 9; since θ only affects α, from eq 25, it only shifts the curve along the log G_c axis and does not change its shape.

On both figures we have compared these theoretical curves with experimental data from the literature. For PMMA the fit to the data is quite good, whereas for PS the theoretical curves are too low at high M_n. This discrepancy, as noted by Wool et al.,[35] is probably caused by the difficulty of producing a sharp crack tip with only a single craze growing from it in high M_n PS. From their welding experiments on PS they estimate that the true high M_n limit for PS is about 400 J/m^2. In PMMA it is much easier to grow a crack with a single craze at the crack tip. The good fit of the model to the G_c data for PMMA down to low molecular weight extends the previous comparison of Hui and Kramer[36] who showed that Döll's[3] measurements of the critical craze width $2h_c$ in high molecular weight PMMA scaled as Σ_{eff}^2, as predicted by eqs 18 and 20.

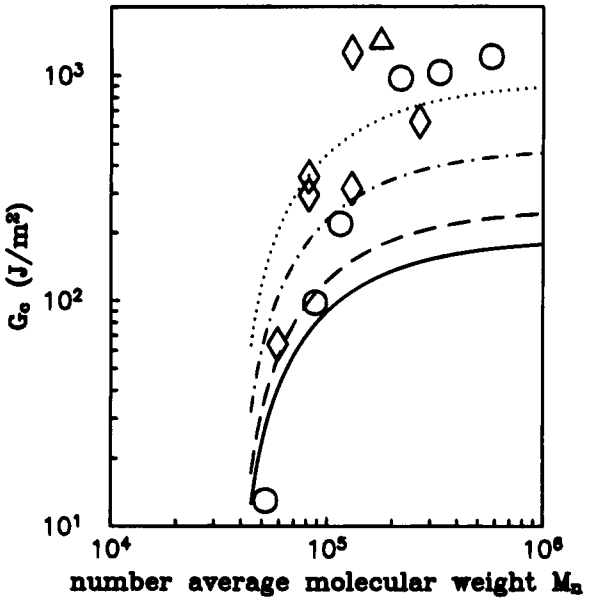

Figure 8. Fracture toughness G_c of polystyrene versus number average molecular weight M_n: (—) for a craze with α = 0.141 (θ = 30); (- - -) for a craze with α = 0.103 (θ = 20); (— · —) for a craze with α = 0.055 (θ = 10); (· · ·) for a craze with α = 0.028 (θ = 5); circles, data of Wool et al.;[35] diamonds, data of Benbow;[47] triangle, data of Berry.[48]

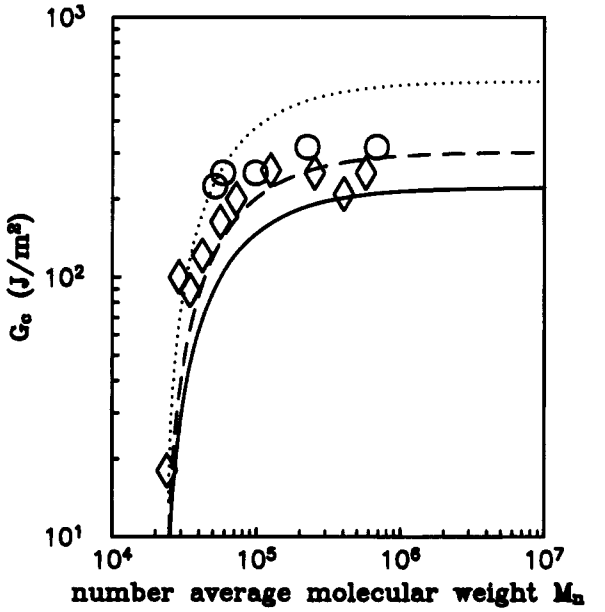

Figure 9. Fracture toughness G_c of poly(methyl methacrylate) versus number average molecular weight M_n: (—) for a craze with α = 0.141 (θ = 30); (- - -) for a craze with α = 0.103 (θ = 20); (· · ·) for a craze with α = 0.055 (θ = 10); circles, data of Berry;[49] diamonds, data of Kusy and Katz.[50]

(2) G_c of Diluted Entanglement Networks. A rather direct method of experimentally testing the Σ_{eff} dependence of G_c is to dilute a high molecular weight polymer with chains of the same polymer which are too short to entangle. While unfortunately there are as yet no such measurements in the literature (craze stability data exist however[7,34]), we make predictions for this dependence in the hope that these will stimulate an experimental test of the model.

Let φ be the volume fraction of the high molecular weight entangled polymer (we will use parameters here appropriate for PS[51]). Then $\nu_e(\varphi) \approx \nu_e(1)\varphi^2$, $M_e(\varphi) \approx M_e(1)/\varphi$, $d_e(\varphi) \approx d_e(1)/\varphi^{1/2}$, and $\Sigma(\varphi) = \Sigma(1)\varphi^{3/2}$ where (1) signifies the property for the pure, high molecular

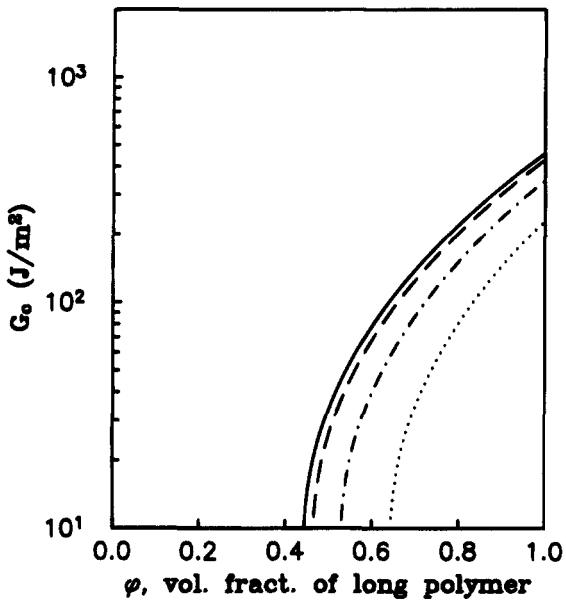

Figure 10. Fracture toughness G_c predicted for entangled polystyrene (PS) chains of molecular weight M diluted with PS too short to entangle: (—) M = 1 000 000; (- - -) M = 500 000; (— · —) M = 200 000; (···) M = 100 000.

weight polymer. If we assume that the strand survival probability is independent of φ (not strictly true since q is a function of d_e[37]), then

$$\Sigma_{eff}(\varphi) = \Sigma_{eff}(1)\varphi^{3/2}\left[1 - \frac{M_e(1)}{q\varphi M_n}\right] \quad (26)$$

We have plotted the G_c versus φ predicted from eqs 25 and 26 in Figure 10 for several different molecular weights of the high molecular weight species. Note that there is a deleterious effect of adding even a relatively small volume fraction of low molecular weight polymer too short to entangle and that G_c approaches zero at about $\varphi \approx 0.44$ even for the highest molecular weight species (M_n = 1 000 000).

(3) Kinetics of Polymer Welding. There have been numerous attempts to relate the $G_c(t)$ determined after two identical homopolymers have been welded above their glass transition temperature for a certain time t to various mechanisms of diffusion and entanglement across the interface.[38-44] It is observed experimentally that G_c scales approximately, but not exactly, as $t^{1/2}$. Usually, a relationship between G_c and some aspect of the diffusing chains is assumed (e.g. the average interpenetration length) and the data are then used to draw conclusions about the diffusion. But in light of the previous discussion, as emphasized previously by Brown, it is the dependence of $\Sigma_{eff}(t)$ on welding time that is actually controlling the time dependence of G_c during welding. At short welding times, G_c is small, implying that only a narrow craze can develop, and thus eq 25 should be used to make the connection between $G_c(t)$ and $\Sigma_{eff}(t)$. We can rewrite eq 25 to explicitly determine $\Sigma_{eff}(t)$, viz.

$$\Sigma_{eff}(t) = \frac{\sigma_d}{f_b\sqrt{1 - \exp(-G^{\ddagger}/G(t))}} \quad (27)$$

where $G^{\ddagger} = 2\pi(1 - v_f)\sigma_d D/\alpha$.

We use eq 27 to extract values of $\Sigma_{eff}(t)$ from the $G(t)$ data reported by Wool et al. The results are plotted in

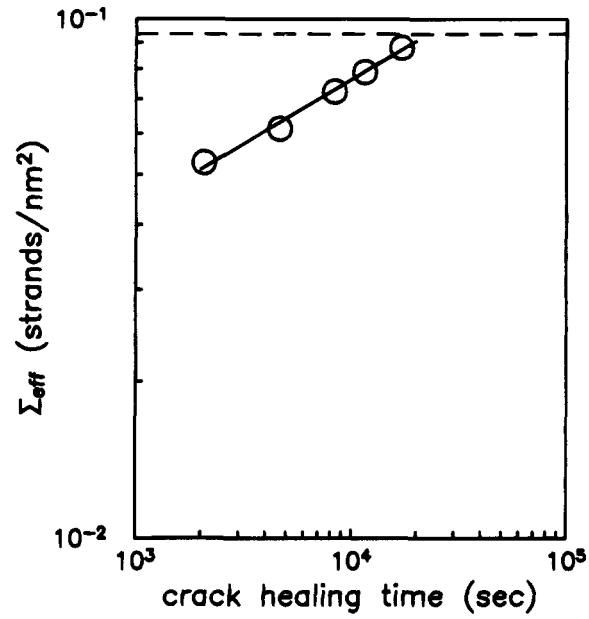

Figure 11. Effective areal chain density [(circles) extracted from the G_c data of Wool et al.[35]] versus crack healing time. The solid line is a linear least squares fit to the data (slope 0.24) while the dashed line represents the predicted Σ_{eff} of the fully healed interface.

Figure 11. The dashed line shows the limiting value of $\Sigma_{eff}(t)$ corresponding to a completely welded homopolymer. The solid line is a linear least squares fit to the data with a slope 0.24 ± 0.02. Future modeling can concentrate on rationalizing the $t^{1/4}$ scaling of $\Sigma_{eff}(t)$ in terms of diffusion models rather than trying to directly predict $G(t)$.

Acknowledgment. C.Y.H., Y.S., and E.J.K. are supported by the Materials Science Center at Cornell, which is funded by the National Science Foundation (DMR-MRL program).

References and Notes

(1) Kramer, E. J. *Adv. Polym. Sci.* **1983**, *52/53*, 1.
(2) Miller, P.; Kramer, E. J. *J. Mater. Sci.* **1991**, *26*, 1459.
(3) Döll, W. *Adv. Polym. Sci.* **1983**, *52/53*, 105.
(4) Wang, W-C. V.; Kramer, E. J. *J. Mater. Sci.* **1982**, *17*, 2013.
(5) Verhuelpen-Heymans, N. *Polym. Eng. Sci.* **1984**, *24*, 809.
(6) Yang, A-C. M.; Kramer, E. J.; Kuo, C. C.; Phoenix, S. L. *Macromolecules* **1986**, *19*, 2010.
(7) Yang, A-C. M.; Kramer, E. J.; Kuo, C. C.; Phoenix, S. L. *Macromolecules* **1986**, *19*, 2020.
(8) Kramer, E. J.; Berger, L. L. *Adv. Polym. Sci.* **1991**, 1.
(9) Brown, H. R. *Macromolecules* **1991**, *24*, 2752.
(10) Miller, P.; Buckley, D. J.; Kramer, E. J. *J. Mater. Sci.* **1991**, *26*, 4445.
(11) Berger, L. L. *Macromolecules* **1989**, *22*, 3162.
(12) Hui, C. Y.; Ruina, A.; Creton, C.; Kramer, E. J. *Macromolecules* **1992**, *25*, 3948.
(13) Duxburg, P. M.; Li, Y. In *Disorder and Fracture*; Charmet, J. C., et al., Eds.; Plenum Press: New York, 1990; Chapter 8, p 141.
(14) Srolovitz, D. J.; Beale, P. D. *J. Am. Ceram. Soc.* **1988**, *71*, 5, 362.
(15) Hassold, G. N.; Srolovitz, D. J. *Phys. Rev. B* **1989**, *39*, 13, 9273.
(16) Meakin, P. *Science* **1991**, *252*, 226.
(17) Kikuchi, A.; Kawai, T.; Suzuki, N. *Comput. Struct.* **1992**, *44*, 469.
(18) Roux, S. In *Statistical Models for the Fracture of Disordered Media*; Hermann, H. J., Roux, S., Eds.; Elsevier Science Publishers B.V.: North Holland, 1990; Vol. 87.
(19) Curtin, W. A.; Arbabi, S. *J. Mater. Res.* **1990**, *5*, 3, 535.
(20) Sahimi, M.; Arbabi, S. *Phys. Rev. B* **1993**, *47*, 2, 713.
(21) Termonia, Y.; Smith, P. *Macromolecules* **1987**, *20*, 835.
(22) Termonia, Y. *J. Mater. Sci.* **1989**, *24*

(23) Monette, L.; Anderson, M. P.; Ling, S.; Grest, G. S. *J. Mater. Sci.* **1992**, *27*, 4393.
(24) Burt, N. J.; Dougill, J. W. *J. Eng. Mech. Div., Am. Soc. Civ. Eng.* **1977**, *103*, 365.
(25) Schlangen, E.; Van Mier, J. G. M. *Int. J. Damage Mech.* **1992**, *1*, 435.
(26) Curtin, W. A.; Scher, H. J. *J. Mater. Res.* **1990**, *5*, 554.
(27) LeSar, R.; Rollett, A. D.; Scher, H. J.; Srolovitz, D. J. *Mater. Sci. Eng.* **1992**, *A155*, 267.
(28) Curtin, W. A.; Futumura, K. *Acta Met. Mater.* **1990**, *38*, 2051.
(29) Jagota, A.; Bennison, S. J. To appear in *Proceedings of a workshop on Breakdown and Nonlinearity in Soft Condensed Matter*; Bardhan, K. K., Chakrabarti, B. K., Hansen, A., Eds.; Springer Verlag Publishers: Berlin, 1994.
(30) Xiao, F.; Curtin, W. A. Submitted to *Macromolecules*.
(31) On one hand, orientation should increase E while on the other the small fibril size may cause an effective decrease in glass transition temperature. Evidence for such a decrease comes from observations of craze fibril coalescence[45] and from direct measurements of the thermal expansion of thin films.[46]
(32) Sih, G. C.; Liebowitz, H. In *Fracture. Mathematical Theory of Brittle Fracture*; Liebowitz, H., Ed.; Academic Press: New York, 1968; Vol. 2, p 67.
(33) Dugdale, D. S. *J. Mech. Phys. Solid* **1960**, *8*, 100.
(34) Berger, L. L. *Macromolecules* **1990**, *23*, 2926.
(35) Wool, R. P.; Yuan, B.-L.; McGarel, O. J. *Polym. Eng. Sci.* **1989**, *29*, 1340.
(36) Hui, C.-Y.; Kramer, E. J. *Use of Plastics and Plastic Composites: Mechanics Issues*; Stokes, V. K., Eds.; ASME Symposium; ASME: Fairfield, NJ, 1993; p 309.
(37) Kuo, C. C.; Phoenix, S. L.; Kramer, E. J. *J. Mater. Sci. Lett.* **1985**, *4*, 459.
(38) Jud, K.; Kausch, H. H. *Polym. Bull.* **1979**, *1*, 697.
(39) Jud, K.; Williams, J. G.; Kausch, H. H. *J. Mater. Sci.* **1981**, *16*, 204.
(40) Wool, R. P.; O'Connor, K. M. *J. Appl. Phys.* **1981**, *52*, 5953.
(41) Prager, S.; Tirrell, M. *J. Chem. Phys.* **1971**, *75*, 5194.
(42) Adolf, D.; Tirrell, M.; Prager, S. *J. Polym. Sci., Polym. Phys.* **1985**, *23*, 413.
(43) deGennes, P.-G. *C. R. Acad. Sci. Paris* **1981**, *292*, 1505.
(44) Mikos, A. G.; Peppas, N. A. *J. Chem. Phys.* **1988**, *88*, 1337.
(45) Yang, A. C. M.; Kramer, E. J. *J. Polym. Sci., Polym. Phys.* **1985**, *23*, 1353.
(46) Keddie, J. L.; Jones, R. A. L.; Cory, R. A. *Europhys. Lett.* **1994**, *27*, 59.
(47) Benbow, J. J. *Pr. Phys. Soc.* **1961**, *78*, 970.
(48) Berry, J. P. *J. Polym. Sci.* **1961**, *50*, 313.
(49) Berry, J. P. *J. Polym. Sci. A* **1964**, *2*, 4069.
(50) Kusy, R. P.; Katz, M. J. *J. Mater. Sci.* **1976**, *11*, 1475.
(51) Graessley, W. W.; Edwards, S. *Polymer* **1981**, *22*, 1329.

MA945091X